photonics

MDPI

Article

Surface-Enhanced Raman Scattering Enabled by a Hybrid Microfiber–Plasmonic Structure with Monolayer MoS_2

Xiaodong Zhao [1], Kaixiang Zhang [1], Chunlei Yu [1,2,*] and Ning Zhou [1,*]

[1] School of Physics and Optoelectronic Engineering, Hangzhou Institute for Advanced Study, University of Chinese Academy of Sciences, Hangzhou 310024, China; zhaoxiaodong22@mails.ucas.ac.cn (X.Z.); zhangkaixiang23@mails.ucas.ac.cn (K.Z.)
[2] Shanghai Institute of Optics and Fine Mechanics, Chinese Academy of Sciences, Shanghai 201800, China
* Correspondence: sdycllcy@163.com (C.Y.); ningzhou@ucas.ac.cn (N.Z.)

Abstract

We demonstrate a mechanism-oriented Surface-Enhanced Raman Scattering (SERS) platform based on a hybrid structure integrating monolayer molybdenum disulfide (MoS_2) and gold nanospheres (AuNSs) on an optical microfiber (MF). The microfiber serves as a whispering-gallery-mode (WGM) microcavity. Monolayer MoS_2, grown directly on the microfiber surface via chemical vapor deposition (CVD), provides a chemically active interface for molecular adsorption and charge-transfer-related chemical enhancement. Subsequently deposited AuNSs couple with the microfiber-supported WGM, leading to the formation of hybrid photonic–plasmonic modes. This coupling results in a narrowed scattering resonance and a localized electromagnetic hotspot near the AuNS–microfiber interface. The combined contribution of electromagnetic enhancement from the microfiber–AuNS hybrid cavity and chemical enhancement from the MoS_2 layer produces discernible Raman enhancement for Rhodamine 6G (R6G) molecules under proof-of-concept measurement conditions. This work provides a useful platform for studying SERS enhancement mediated by hybrid photonic–plasmonic modes and offers guidance for the future development of optimized fiber-based SERS sensors.

Keywords: surface-enhanced Raman scattering; two-dimensional material; MoS_2; microfiber; hybrid photonic–plasmonic mode

1. Introduction

Raman spectroscopy is a powerful analytical technique that provides distinct vibrational fingerprints of molecules, enabling non-destructive and label-free chemical identification. It has been widely applied in materials science, chemistry, biology, and medicine. However, the intrinsically low efficiency of spontaneous Raman scattering severely limits its sensitivity, making the detection of trace analytes challenging in practical applications.

Surface-enhanced Raman scattering (SERS) has been extensively investigated as an effective strategy to overcome the sensitivity limitation of conventional Raman spectroscopy [1–5]. The enhancement of Raman signals in SERS is generally attributed to two primary mechanisms: electromagnetic enhancement (EME) and chemical enhancement (CE). EME arises from the strong localization and amplification of electromagnetic fields near plasmonic nanostructures, typically composed of noble metals such as gold or silver. CE, which usually provides a smaller contribution, originates from charge–transfer interactions between the analyte molecules and the substrate, leading to modifications in molecular polarizability and Raman scattering cross-sections [6,7].

Check for updates

Received: 6 May 2026
Revised: 5 June 2026
Accepted: 11 June 2026
Published: 15 June 2026

Copyright: © 2026 by the authors. Licensee MDPI, Basel, Switzerland. This article is an open access article distributed under the terms and conditions of the Creative Commons Attribution (CC BY) license.

To further improve SERS performance, hybrid substrates that combine plasmonic nanostructures with two-dimensional (2D) materials have attracted increasing attention [6,8]. Among various 2D materials, molybdenum disulfide (MoS_2) has emerged as a promising component owing to its atomically thin structure, tunable electronic properties, and large surface area [9]. Monolayer MoS_2 has been reported to contribute to SERS enhancement through charge–transfer-related chemical enhancement and excitonic-resonance-related effects, while also suppressing fluorescence background and improving signal stability in Raman measurements [10–12].

Optical microfibers with diameters comparable to the wavelength of light provide a versatile platform for photonic sensing applications due to their strong evanescent fields, low propagation loss, and flexible geometry [13]. The circular cross-section of a microfiber naturally supports whispering gallery modes (WGMs), in which light circulates near the fiber surface via total internal reflection, enabling enhanced light–matter interaction [14,15]. These characteristics make optical microfibers attractive building blocks for compact and integrated photonic devices. Recent studies have shown that coupling plasmonic nanoparticles to microfiber-based WGM cavities can give rise to hybrid photonic–plasmonic modes [16–23]. In such systems, the broadband localized surface plasmon resonance of a metallic nanoparticle interacts with the narrow-band photonic resonance of the microfiber, leading to a pronounced narrowing of the plasmon resonance linewidth. This linewidth compression reflects improved optical coherence and prolonged photon lifetime in the hybrid system, which can significantly enhance the local electromagnetic field intensity near the nanoparticle.

In this work, we demonstrate a hybrid SERS platform that integrates an optical microfiber, gold nanospheres, and a monolayer of MoS_2 (Figure 1a). In this architecture, the optical microfiber functions as a whispering gallery mode cavity that couples with the localized surface plasmon resonance of the gold nanospheres, resulting in a pronounced narrowing of the plasmon resonance linewidth and the formation of a highly confined electromagnetic hotspot. The monolayer MoS_2 serves as an active chemical enhancement layer that facilitates charge–transfer interactions with probe molecules and provides a favorable adsorption interface. This hybrid configuration enables us to investigate how microfiber-mediated photonic–plasmonic coupling and MoS_2-assisted chemical enhancement jointly contribute to the Raman enhancement of Rhodamine 6G (R6G) molecules.

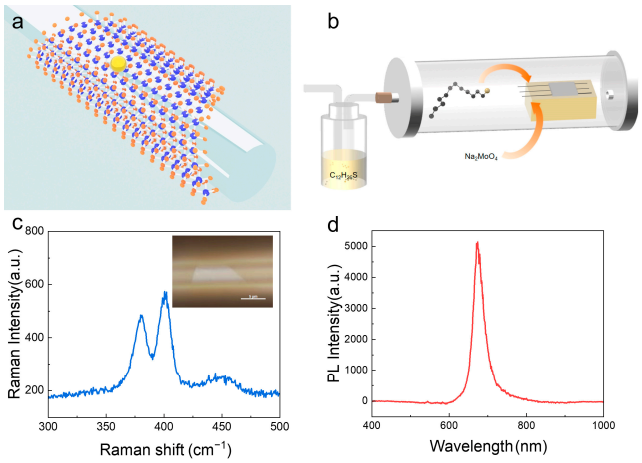


Figure 1. Fabrication and characterization of monolayer MoS_2 on an optical microfiber. (**a**) Schematic illustration of the hybrid SERS substrate structure, composed of a microfiber, a monolayer of MoS_2, and a gold nanosphere. (**b**) Schematic diagram of the CVD setup used for growing MoS_2 on the microfiber. (**c**) Raman spectrum of the MoS_2 film on the microfiber; the inset shows an optical microscope image of the microfiber after MoS_2 growth. (**d**) PL spectrum of the MoS_2 film on the microfiber.

2. Experimental Methods

2.1. Microfiber Fabrication and MoS_2 Synthesis

Optical microfibers were fabricated by tapering standard single-mode optical fibers using a flame-heated pulling technique [24–27]. The diameter of the microfiber waist was controlled in real time to ensure low optical loss and stable mode guidance. The resulting microfibers exhibit strong evanescent fields and naturally support whispering gallery modes, which provide an effective optical cavity for coupling with plasmonic nanoparticles. Monolayer MoS_2 was synthesized directly on the surface of the microfiber through a chemical vapor deposition (CVD) method, as schematically shown in Figure 1b. Sodium molybdate (Na_2MoO_4) solution was used as the molybdenum precursor, and 1-dodecanethiol ($C_{12}H_{26}S$) served as the sulfur source. Prior to growth, the microfiber was treated with oxygen plasma for 60 s to enhance the surface hydrophilicity. A small amount of Na_2MoO_4 precursor solution was then drop-cast onto the microfiber and dried in air. The microfiber was placed at the center of a quartz tube furnace, while the sulfur precursor was positioned upstream. The system was purged with argon for 30 min, and the furnace was subsequently heated to 830 °C at a rate of 20 °C/min. The growth was maintained for 40 min, during which the sulfur vapor reacted with the molybdenum precursor on the microfiber surface. After growth, the furnace was cooled naturally to room temperature under an argon atmosphere. This CVD process enables the formation of a conformal MoS_2 monolayer coating on the cylindrical microfiber surface, providing an active semiconductor interface for chemical enhancement in the hybrid SERS structure.

2.2. Fabrication and Characterization of the Hybrid SERS Substrate

The hybrid SERS substrate was prepared by depositing citrate-stabilized gold nanospheres (AuNSs) onto the MoS_2-coated microfiber. The 80 nm AuNSs were chosen because their visible-range plasmonic scattering response is sufficiently strong for dark-field identification and optical coupling measurements [28,29]. The MoS_2-coated microfiber was immersed in a diluted aqueous suspension of 80 nm AuNSs (X-nanogold Ltd., Jiaxing, China) for several minutes and then removed and dried in air. The AuNSs were deposited onto the MoS_2-coated microfiber through a drying-assisted physical adsorption process. The attachment is mainly attributed to capillary forces during solvent evaporation and van der Waals interactions, while possible electrostatic interactions may also contribute. In the AuNS/MoS_2/microfiber geometry, the monolayer MoS_2 acts as an atomically thin spacer between the AuNS and the microfiber surface, forming a MoS_2-defined nanoscale gap that supports near-field coupling.

The morphology of the resulting structure was examined using scanning electron microscopy (SEM). The optical scattering response of individual Au nanospheres coupled to the microfiber was measured using a dark-field spectroscopy setup, in which white light from a supercontinuum source illuminated the sample, and the scattered signal was collected by a 50× objective lens and analyzed by a spectrometer (QE Pro, Ocean Optics, Dunedin, FL, USA). Finite-difference time-domain (FDTD) simulations were carried out to calculate the electromagnetic field distribution around a single Au nanosphere coupled to the microfiber cavity. These simulations provide insight into the formation of the localized electromagnetic hotspot responsible for Raman enhancement.

For Raman/SERS measurements, the hybrid structures and control samples were immersed in a 10^{-6} M ethanol solution of R6G for 30 min to allow molecular adsorption. After drying, Raman spectra were collected using a 532 nm excitation laser with a laser power of 3 mW and an exposure time of 5 s. The scattered light was collected using the same objective and detected by a monochromator (Omni-A3004i, Zolix, Beijing, China) equipped with an electron-multiplying CCD (EMCCD) (DU-888, Andor, Belfast, UK). Because the

samples include curved microfiber structures, the exact laser spot size and local power density on the microfiber surface are difficult to determine accurately under the present optical configuration. Therefore, the directly controlled experimental parameters, including excitation wavelength, laser power, and exposure time, are reported here.

3. Results and Discussion

3.1. Characterization of CVD-Grown Monolayer MoS_2 on Microfiber

The successful synthesis of monolayer MoS_2 on the cylindrical microfiber surface is essential for constructing the hybrid SERS platform. After the CVD process, optical microscopy reveals that monolayer MoS_2 is continuously grown on the microfiber over a well-defined region of the fiber waist (inset of Figure 1c). Although the MoS_2 layer does not necessarily cover the entire fiber circumference, it forms a conformal and continuous coating along the cylindrical surface, consistent with previous reports on CVD-grown monolayer MoS_2 on optical microfibers [30].

To verify the layer thickness and crystal quality, Raman and photoluminescence (PL) spectroscopy were performed on the MoS_2-coated microfiber. Figure 1c shows the characteristic Raman spectrum of MoS_2 obtained from the microfiber surface. Two prominent peaks are observed: the in-plane E^1_{2g} mode at ~385 cm^{-1} and the out-of-plane A^1_g mode at ~405 cm^{-1}. The frequency difference (Δk) between these two peaks is approximately 20 cm^{-1}, which is consistent with monolayer MoS_2 grown on curved or strained substrates [25].

The PL spectrum shows a pronounced emission peak centered at ~673 nm, which can be assigned to the A-exciton-related direct-band-gap emission of monolayer MoS_2. Since monolayer MoS_2 exhibits much stronger PL than multilayer MoS_2 owing to the transition from an indirect to a direct band gap [31], the strong PL emission, together with the Raman-mode separation of approximately 20 cm^{-1}, supports the predominantly monolayer nature of the synthesized MoS_2. The PL peak position is also consistent with previous reports on monolayer MoS_2 grown on silica micro/nanofibers [30]. In this hybrid structure, the monolayer MoS_2 primarily provides a chemically active and uniform adsorption interface. Its role is to facilitate photo-induced charge–transfer interactions with analyte molecules and to improve the reproducibility of Raman signals, rather than forming an additional optical resonance within the microfiber–plasmonic cavity.

3.2. Morphological and Optical Characterization of the Hybrid Microfiber–Plasmonic Structure

Figure 2a presents a dark-field optical microscope image of the MoS_2-coated microfiber after Au nanosphere deposition. The microfiber is weakly visible, while individual Au nanospheres appear as bright scattering spots, confirming their successful attachment to the fiber surface. A representative SEM image (Figure 2b) further shows a single 80 nm Au nanosphere located on the microfiber. The MoS_2 monolayer underneath the nanoparticle is not resolved in SEM but has been confirmed by Raman and PL characterization in Section 3.1. It should be noted that the relatively low AuNS loading density was intentionally adopted in this work to resolve isolated AuNS–microfiber coupling events. This configuration minimizes interparticle coupling, aggregation, and ensemble averaging, thereby allowing a clearer correlation between the narrowed scattering resonance, the simulated electromagnetic hotspot, and the observed Raman enhancement. Therefore, the present structure is designed as a mechanism-oriented hybrid microfiber–plasmonic SERS platform rather than an optimized high-density SERS substrate.

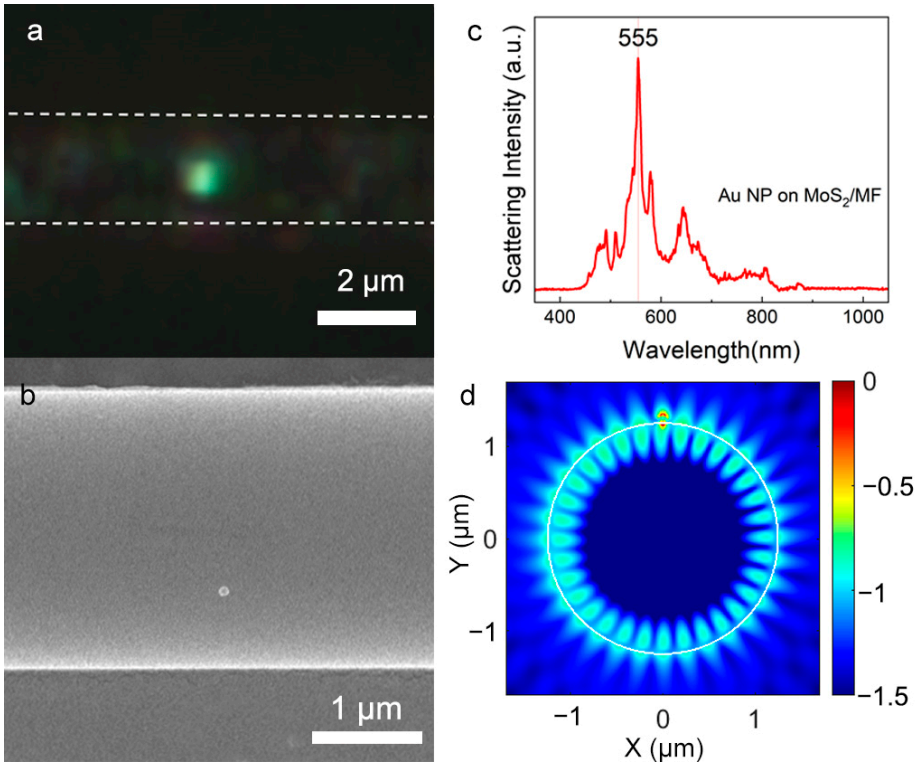


Figure 2. Morphological and optical properties of the hybrid microfiber–MoS_2–AuNS structure. (**a**) Dark-field optical microscope image showing individual Au nanospheres as bright scattering spots on the microfiber. The white dashed line represents the contour of the microfiber to the figure caption. (**b**) Representative SEM image of an individual 80 nm Au nanosphere located on the surface of a MoS_2-coated microfiber with a diameter of approximately 2.5 μm. The isolated particle configuration was used to study the elementary AuNS–microfiber coupling unit. (**c**) Experimental scattering spectrum of an individual Au nanosphere coupled to the microfiber, showing a spectrally narrowed resonance arising from the formation of a hybrid photonic–plasmonic cavity mode. (**d**) Normalized electric-field intensity distribution of the Au nanosphere–microfiber system at the resonance wavelength, revealing a localized electromagnetic hotspot in the nanoparticle–fiber gap region.

The optical scattering response of the hybrid structure is governed by the interaction between the localized surface plasmon resonance (LSPR) of the Au nanospheres and the whispering gallery modes (WGMs) of the microfiber cavity. Figure 2c shows the measured scattering spectrum of an individual Au nanosphere coupled to the microfiber. A distinct resonant peak is observed, which is considerably narrower than the LSPR linewidth of the same Au nanospheres deposited on a flat glass substrate [28,29]. This linewidth narrowing originates from the formation of a hybrid photonic–plasmonic cavity mode, where the plasmonic resonance of the Au nanosphere couples to the microfiber WGM. Such coupling prolongs the photon lifetime in the hybrid cavity and leads to an enhanced and spectrally compressed electromagnetic response near the nanoparticle [16–23]. The presence of the MoS_2 monolayer does not introduce an additional optical resonance but modifies the local dielectric environment and provides a uniform and chemically active interface for molecular adsorption.

To visualize the electromagnetic enhancement in this hybrid cavity, FDTD simulations were performed. The calculated electric-field intensity distribution at the resonance wavelength is shown in Figure 2d. A strongly confined electromagnetic hotspot is formed in the nanogap region between the Au nanosphere and the microfiber surface. In the AuNS/MoS_2/microfiber geometry, the monolayer MoS_2 also serves as an atomically thin spacer between the AuNS and the microfiber surface. The resulting MoS_2-defined nanoscale

gap maintains near-field coupling between the AuNS plasmon resonance and the microfiber cavity mode, while providing a chemically active interface for charge–transfer-related SERS enhancement. This highly localized field is responsible for the dominant electromagnetic enhancement observed in subsequent SERS measurements.

3.3. SERS Performance and Enhancement Mechanism

The Raman response of the hybrid microfiber-MoS_2-AuNS structure was evaluated using R6G as a probe molecule. Figure 3a compares the Raman spectra obtained from AuNS + MoS_2 + MF, MoS_2 + MF, AuNS + MF, bare MF, AuNS + MoS_2 + SiO_2/Si, and MoS_2 + SiO_2/Si after incubation in a 10^{-6} M R6G solution. Compared with the microfiber-based controls, the AuNS + MoS_2 + MF structure shows discernible R6G Raman features under the present proof-of-concept measurement conditions, indicating the combined contribution of localized electromagnetic enhancement from AuNS–microfiber coupling and MoS_2-assisted chemical enhancement.

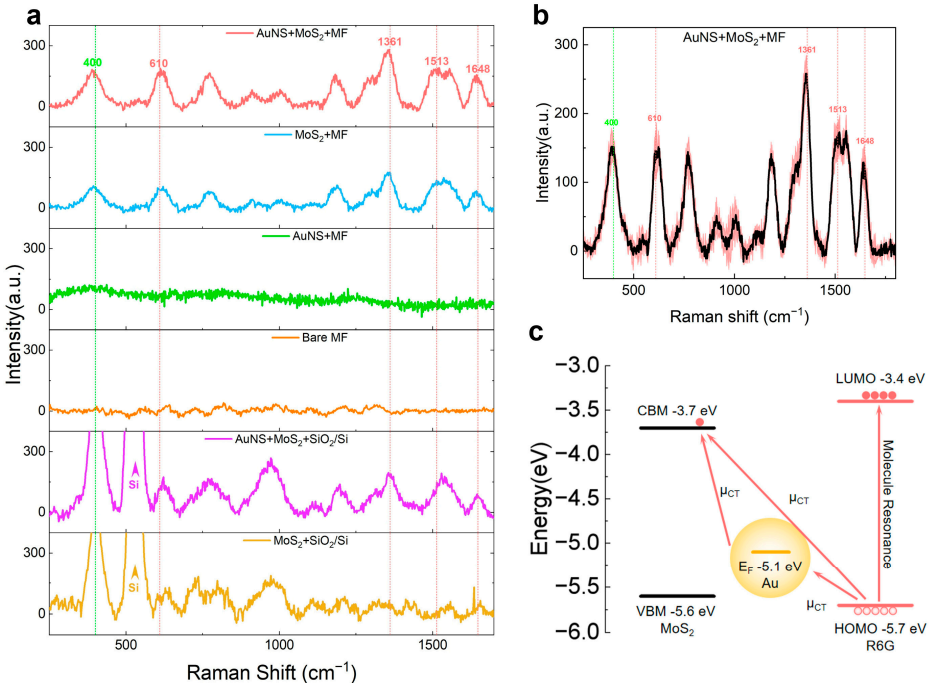


Figure 3. SERS performance and enhancement mechanism. (**a**) Comparative Raman spectra of 10^{-6} M R6G collected from the hybrid structure (AuNS + MoS_2 + MF), MoS_2-coated microfiber (MoS_2 + MF), AuNS-modified microfiber (AuNS + MF), bare microfiber, AuNS + MoS_2 on a planar SiO_2/Si substrate (AuNS + MoS_2 + SiO_2/Si), and MoS_2 on a planar SiO_2/Si substrate (MoS_2 + SiO_2/Si). All spectra are plotted using the original Raman intensity scale. The measurement was performed using a 532 nm laser with a power of 3 mW and an exposure time of 5 s. (**b**) Repeated Raman measurements of 10^{-6} M R6G collected from the AuNS + MoS_2 + MF structure. The shaded envelope represents the spectral variation range obtained from repeated measurements. (**c**) Schematic energy-level diagram illustrating the chemical enhancement mechanism. Under 532 nm excitation, resonance-assisted charge transfer may occur between R6G and monolayer MoS_2, while Au-mediated hot-electron transfer may also contribute locally near the AuNSs. These processes can increase the molecular polarizability and contribute to chemical enhancement.

The AuNS + MF and bare MF controls show no obvious R6G Raman peaks under the present measurement conditions. For the bare microfiber, the absence of both plasmonic electromagnetic enhancement and MoS_2-assisted chemical enhancement makes the normal Raman signal of 10^{-6} M R6G too weak to be clearly detected. For the AuNS + MF sample, the low AuNS loading density and the limited hotspot volume around isolated AuNSs

make the detected signal strongly dependent on whether R6G molecules are located within the near-field region. Nonuniform drying and limited molecular adsorption on the curved microfiber surface may therefore lead to weak or undetectable Raman signals. In contrast, the AuNS + MoS_2 + MF structure provides both localized electromagnetic enhancement and a chemically active MoS_2 interface, resulting in more discernible R6G Raman features.

The planar AuNS + MoS_2 + SiO_2/Si and MoS_2 + SiO_2/Si controls exhibit stronger Raman features than the microfiber-based controls. This difference may arise partly from optical interference effects in the approximately 300 nm SiO_2/Si substrate, which can enhance the local excitation field and Raman collection efficiency near the surface [32,33]. In addition, the planar substrate provides a larger and flatter surface for R6G adsorption and optical collection. Therefore, the absolute Raman intensity from the planar SiO_2/Si controls should not be directly compared with that from the microfiber geometry without considering substrate interference and collection-geometry effects.

Although high-density AuNS coverage is generally desirable for practical SERS substrates because it can provide more plasmonic hotspots and better spatial reproducibility, the present work focuses on the mechanism of SERS enhancement in a hybrid microfiber–plasmonic cavity. The low-density AuNS configuration allows the contribution of the AuNS–microfiber hybrid mode to be more clearly identified. Therefore, the observed Raman enhancement should be understood as a proof-of-concept demonstration of hybrid-mode-mediated SERS enhancement, rather than as the optimized performance of a high-density analytical SERS substrate.

The dominant enhancement mechanism in this system is electromagnetic enhancement (EME), arising from the hybrid photonic–plasmonic cavity formed by the coupling between the Au nanospheres and the microfiber WGMs [16–23]. The spectral linewidth narrowing observed in the scattering spectra indicates prolonged photon lifetime and enhanced optical coherence in the hybrid cavity. As shown by the FDTD simulation (Figure 2d), this coupling generates a strongly confined electromagnetic hotspot in the nanoparticle–fiber gap region. The Raman enhancement scales approximately with the fourth power of the local field intensity, leading to the pronounced signal amplification for molecules located within this hotspot [1–5].

In addition to the electromagnetic enhancement (EME), the monolayer MoS_2 provides a crucial contribution through chemical enhancement (CE) [7,10–12]. The mechanism of CE is schematically illustrated by the energy-level diagram in Figure 3c, which depicts a photo-induced charge transfer process. The highest occupied molecular orbital (HOMO) and lowest unoccupied molecular orbital (LUMO) of R6G are estimated to be at approximately −5.7 eV and −3.4 eV, respectively. Monolayer MoS_2 has a valence band maximum (VBM) at around −5.6 eV and a conduction band minimum (CBM) at −3.7 eV. Under excitation with a 532 nm laser (2.33 eV), R6G molecules can be resonantly excited from the HOMO to the LUMO level [34,35]. The energy-level alignment between R6G and monolayer MoS_2 can further facilitate photo-induced charge transfer at the molecule–MoS_2 interface, which can modify the molecular polarizability and increase the Raman scattering cross-section. In the localized region near AuNSs, Au-mediated hot-electron transfer may also participate in the interfacial charge-transfer process. This CE pathway works in concert with the EME provided by the microfiber–plasmonic cavity, further contributing to the overall Raman enhancement.

The MF + MoS_2 control experiment exhibits only a weak Raman response, indicating that CE alone provides a limited enhancement. However, when combined with the strong EME from the plasmonic hotspot, the contribution of CE becomes more apparent in the total observed Raman response. In addition, the MoS_2 layer provides a chemically active adsorption interface that promotes molecular adsorption compared with the bare microfiber surface. Therefore, the observed Raman enhancement originates from the com-

bined contribution of electromagnetic enhancement from the microfiber–plasmonic cavity and MoS_2-assisted resonance-related chemical enhancement.

4. Conclusions

In summary, we have demonstrated a proof-of-concept and mechanism-oriented hybrid microfiber–plasmonic SERS platform integrating an optical microfiber, citrate-stabilized AuNSs, and a monolayer of MoS_2. The optical microfiber provides a WGM cavity that couples with the localized surface plasmon resonance of the AuNSs, leading to a narrowed hybrid photonic–plasmonic resonance and a localized electromagnetic hotspot near the AuNS–microfiber interface. The monolayer MoS_2 grown on the microfiber surface acts as an atomically thin spacer and a chemically active adsorption interface, contributing to resonance-assisted charge–transfer-related chemical enhancement. The observed Raman response of R6G results from the combined contribution of electromagnetic enhancement from the microfiber–plasmonic cavity and MoS_2-assisted chemical enhancement. The present study should be regarded as a proof-of-concept demonstration of hybrid-mode-mediated SERS enhancement rather than an optimized high-density analytical SERS substrate. Further optimization, including increasing AuNS coverage, improving nanoparticle-distribution uniformity, controlling molecular adsorption, and performing quantitative enhancement-factor and limit-of-detection analyses, will be necessary for application-oriented high-performance fiber-based SERS sensing.

Author Contributions: Conceptualization, X.Z. and N.Z.; methodology, X.Z., K.Z. and N.Z.; validation, X.Z. and K.Z.; formal analysis, X.Z.; writing—original draft preparation, X.Z., K.Z. and N.Z.; writing—review and editing, N.Z. and C.Y.; visualization, X.Z.; supervision, N.Z. and C.Y.; project administration, N.Z. and C.Y.; funding acquisition, N.Z. All authors have read and agreed to the published version of the manuscript.

Funding: This work was supported by the National Natural Science Foundation of China (62005236) and the Research Funds of Hangzhou Institute for Advanced Study, UCAS.

Data Availability Statement: The data that support the findings of this study are available from the corresponding author upon reasonable request.

Conflicts of Interest: The authors declare no conflicts of interest.

Abbreviations

The following abbreviations are used in this manuscript:

SERS	Surface-Enhanced Raman Scattering
MF	Microfiber
AuNSs	Gold nanospheres
WGM	Whispering gallery mode
CVD	Chemical vapor deposition
EME	Electromagnetic enhancement
CM	Chemical enhancement
SEM	Scanning electron microscopy
FDTD	Finite-difference time-domain
LSPR	Localized surface plasmon resonance
2D	Two-dimension
PICT	Photo-induced charge transfer
HOMO	Highest occupied molecular orbital
LUMO	Lowest unoccupied molecular orbital
VBM	Valence band maximum
CBM	Conduction band minimum

References

1. Wang, X.; Huang, S.; Hu, S.; Yan, S.; Ren, B. Fundamental understanding and applications of plasmon-enhanced Raman spectroscopy. *Nat. Rev. Phys.* **2020**, *2*, 253–271. [CrossRef]
2. Langer, J.; Jimenez De Aberasturi, D.; Aizpurua, J.; Alvarez-Puebla, R.A.; Auguié, B.; Baumberg, J.J.; Bazan, G.C.; Bell, S.E.J.; Boisen, A.; Brolo, A.G.; et al. Present and Future of Surface-Enhanced Raman Scattering. *ACS Nano* **2020**, *14*, 28–117. [CrossRef] [PubMed]
3. Wang, H.; You, E.; Panneerselvam, R.; Ding, S.; Tian, Z. Advances of surface-enhanced Raman and IR spectroscopies: From nano/microstructures to macro-optical design. *Light Sci. Appl.* **2021**, *10*, 161. [CrossRef] [PubMed]
4. Itoh, T.; Procházka, M.; Dong, Z.; Ji, W.; Yamamoto, Y.S.; Zhang, Y.; Ozaki, Y. Toward a New Era of SERS and TERS at the Nanometer Scale: From Fundamentals to Innovative Applications. *Chem. Rev.* **2023**, *123*, 1552–1634. [CrossRef]
5. Ma, H.; Pan, S.; Wang, W.; Yue, X.; Xi, X.; Yan, S.; Wu, D.; Wang, X.; Liu, G.; Ren, B. Surface-Enhanced Raman Spectroscopy: Current Understanding, Challenges, and Opportunities. *ACS Nano* **2024**, *18*, 14000–14019. [CrossRef]
6. Thakur, A.; Singh, R.; Yadav, V.; Siddhanta, S.; Jayarmaulu, K. Advancing SERS Applications of 2D Materials through the Interplay of Rational Design and Structure-Property Relationships. *Small Methods* **2025**, *9*, 2402056. [CrossRef] [PubMed]
7. Liu, Y.; Ma, H.; Han, X.X.; Zhao, B. Metal–semiconductor heterostructures for surface-enhanced Raman scattering: Synergistic contribution of plasmons and charge transfer. *Mater. Horiz.* **2021**, *8*, 370–382. [CrossRef]
8. Yang, H.; Mo, H.; Zhang, J.; Hong, L.; Li, Z. Observation of single-molecule Raman spectroscopy enabled by synergic electromagnetic and chemical enhancement. *PhotoniX* **2024**, *5*, 3. [CrossRef]
9. Yang, X.; Li, B. Monolayer MoS_2 for nanoscale photonics. *Nanophotonics* **2020**, *9*, 1557–1577. [CrossRef]
10. Sun, L.; Hu, H.; Zhan, D.; Yan, J.; Liu, L.; Teguh, J.S.; Yeow, E.K.L.; Lee, P.S.; Shen, Z. Plasma Modified MoS_2 Nanoflakes for Surface Enhanced Raman Scattering. *Small* **2014**, *10*, 1090–1095. [CrossRef] [PubMed]
11. Muehlethaler, C.; Considine, C.R.; Menon, V.; Lin, W.-C.; Lee, Y.-H.; Lombardi, J.R. Ultrahigh Raman Enhancement on Monolayer MoS_2. *ACS Photonics* **2016**, *3*, 1164–1169. [CrossRef]
12. Sun, H.; Yao, M.; Song, Y.; Zhu, L.; Dong, J.; Liu, R.; Li, P.; Zhao, B.; Liu, B. Pressure-Induced SERS Enhancement in a MoS_2/Au/R6G System by a Two-Step Charge Transfer Process. *Nanoscale* **2019**, *11*, 21493–21501. [CrossRef]
13. Zhang, J.; Fang, H.; Wang, P.; Fang, W.; Zhang, L.; Guo, X.; Tong, L. Optical microfiber or nanofiber: A miniature fiber-optic platform for nanophotonics. *Photonics Insights* **2024**, *3*, R02. [CrossRef]
14. Sumetsky, M. Mode localization and the Q-factor of a cylindrical microresonator. *Opt. Lett.* **2010**, *35*, 2385–2387. [CrossRef]
15. Sharma, I.; Sumetsky, M. Widely FSR tunable high Q-factor microresonators formed at the intersection of straight optical fibers. *Optica* **2025**, *12*, 890–893. [CrossRef]
16. Fu, Y.; Qing, Y.M.; Li, Z.; Zayats, A.V.; Lei, D. Tale of Two Resonances: Waveguide–Plasmon Coupling and High Q-Factor Engineering on the Nanoscale. *ACS Photonics* **2023**, *10*, 2–12. [CrossRef]
17. Zhou, N.; Yang, Y.; Guo, X.; Gong, J.; Shi, Z.; Yang, Z.; Wu, H.; Gao, Y.; Yao, N.; Fang, W.; et al. Strong mode coupling-enabled hybrid photon-plasmon laser with a microfiber-coupled nanorod. *Sci. Adv.* **2022**, *8*, eabn2026. [CrossRef] [PubMed]
18. Jin, Y.; Yang, L.; Pan, C.; Shi, Z.; Cui, B.; Xu, P.; Yang, Y.; Zhou, N.; Guo, X.; Wang, P.; et al. Strong coupling of a plasmonic nanoparticle to a semiconductor nanowire. *Nanophotonics* **2021**, *10*, 2875–2881. [CrossRef]
19. Ai, Q.; Sterl, F.; Zhang, H.; Wang, J.; Giessen, H. Giant Second Harmonic Generation Enhancement in a High-Q Doubly Resonant Hybrid Plasmon–Fiber Cavity System. *ACS Nano* **2021**, *15*, 19409–19417. [CrossRef] [PubMed]
20. Zhou, N.; Wang, P.; Shi, Z.X.; Gao, Y.X.; Yang, Y.X.; Wang, Y.P.; Xie, Y.; Cai, D.W.; Guo, X.; Zhang, L.; et al. Au nanorod-coupled microfiber optical humidity sensors. *Opt. Express* **2019**, *27*, 8180–8185. [PubMed]
21. Ai, Q.; Gui, L.; Paone, D.; Metzger, B.; Mayer, M.; Weber, K.; Fery, A.; Giessen, H. Ultranarrow Second-Harmonic Resonances in Hybrid Plasmon-Fiber Cavities. *Nano Lett.* **2018**, *18*, 5576–5582. [CrossRef]
22. Gu, F.; Zhang, L.; Zhu, Y.; Zeng, H. Free-space coupling of nanoantennas and whispering-gallery microcavities with narrowed linewidth and enhanced sensitivity. *Laser Photon. Rev.* **2015**, *9*, 682–688. [CrossRef]
23. Wang, P.; Wang, Y.P.; Yang, Z.Y.; Guo, X.; Lin, X.; Yu, X.C.; Xiao, Y.F.; Fang, W.; Zhang, L.; Lu, G.W.; et al. Single-Band 2-nm-Line-Width Plasmon Resonance in a Strongly Coupled Au Nanorod. *Nano Lett.* **2015**, *15*, 7581–7586. [CrossRef] [PubMed]
24. Kang, Y.; Gong, J.; Xu, Y.; Yao, N.; Fang, W.; Guo, X.; Tong, L. Ultrahigh-Precision Diameter Control of Nanofiber Using Direct Mode Cutoff Feedback. *IEEE Photonics Technol. Lett.* **2020**, *32*, 219–222. [CrossRef]
25. Yao, N.; Linghu, S.; Xu, Y.; Zhu, R.; Zhou, N.; Gu, F.; Zhang, L.; Fang, W.; Ding, W.; Tong, L. Ultra-Long Subwavelength Micro/Nanofibers With Low Loss. *IEEE Photonics Technol. Lett.* **2020**, *32*, 1069–1072. [CrossRef]
26. Xu, Y.; Fang, W.; Tong, L. Real-time control of micro/nanofiber waist diameter with ultrahigh accuracy and precision. *Opt. Express* **2017**, *25*, 10434–10440. [CrossRef]
27. Tong, L.; Gattass, R.R.; Ashcom, J.B.; He, S.; Lou, J.; Shen, M.; Maxwell, I.; Mazur, E. Subwavelength-diameter silica wires for low-loss optical wave guiding. *Nature* **2003**, *426*, 816–819. [CrossRef]

28. Jain, P.K.; Lee, K.S.; El-Sayed, I.H.; El-Sayed, M.A. Calculated Absorption and Scattering Properties of Gold Nanoparticles of Different Size, Shape, and Composition: Applications in Biological Imaging and Biomedicine. *J. Phys. Chem. B* **2006**, *110*, 7238–7248. [CrossRef]
29. Anderson, L.J.E.; Mayer, K.M.; Fraleigh, R.D.; Yang, Y.; Lee, S.; Hafner, J.H. Quantitative Measurements of Individual Gold Nanoparticle Scattering Cross Sections. *J. Phys. Chem. C* **2010**, *114*, 11127–11132. [CrossRef]
30. Liao, F.; Yu, J.; Gu, Z.; Yang, Z.; Hasan, T.; Linghu, S.; Peng, J.; Fang, W.; Zhuang, S.; Gu, M.; et al. Enhancing monolayer photoluminescence on optical micro/nanofibers for low-threshold lasing. *Sci. Adv.* **2019**, *5*, eaax7398. [CrossRef] [PubMed]
31. Splendiani, A.; Sun, L.; Zhang, Y.; Li, T.; Kim, J.; Chim, C.-Y.; Galli, G.; Wang, F. Emerging Photoluminescence in Monolayer MoS_2. *Nano Lett.* **2010**, *10*, 1271–1275. [CrossRef]
32. Vančo, Ľ.; Kotlár, M.; Kadlečíková, M.; Vretenár, V.; Vojs, M.; Kováč, J. Interference-Enhanced Raman Scattering in SiO_2/Si Structures Related to Reflectance. *J. Raman Spectrosc.* **2019**, *50*, 1502–1509. [CrossRef]
33. Van Velson, N.; Zobeiri, H.; Wang, X. Thickness-Dependent Raman Scattering from Thin-Film Systems. *J. Phys. Chem. C* **2023**, *127*, 2995–3004. [CrossRef]
34. Dieringer, J.A.; Wustholz, K.L.; Masiello, D.J.; Camden, J.P.; Kleinman, S.L.; Schatz, G.C.; Van Duyne, R.P. Surface-Enhanced Raman Excitation Spectroscopy of a Single Rhodamine 6G Molecule. *J. Am. Chem. Soc.* **2009**, *131*, 849–854. [CrossRef] [PubMed]
35. Ujihara, M.; Dang, N.M.; Imae, T. Surface-Enhanced Resonance Raman Scattering of Rhodamine 6G in Dispersions and on Films of Confeito-Like Au Nanoparticles. *Sensors* **2017**, *17*, 2563. [CrossRef] [PubMed]

Disclaimer/Publisher's Note: The statements, opinions and data contained in all publications are solely those of the individual author(s) and contributor(s) and not of MDPI and/or the editor(s). MDPI and/or the editor(s) disclaim responsibility for any injury to people or property resulting from any ideas, methods, instructions or products referred to in the content.